In situ electro-mechanical experiments and mechanics modeling of tensile cracking in indium tin oxide thin films on polyimide substrates

Cheng Peng,[1] Zheng Jia,[2] Dan Bianculli,[1] Teng Li,[2,a)] and Jun Lou[1,b)]
[1]*Department of Mechanical Engineering and Materials Science, Rice University, Houston, Texas 77005, USA*
[2]*Department of Mechanical Engineering and Maryland NanoCenter, University of Maryland, College Park, Maryland 20742, USA*

(Received 25 February 2011; accepted 17 April 2011; published online 27 May 2011)

Indium tin oxide (ITO) thin films supported by polymer substrates have been widely used as transparent electrodes/interconnects in flexible electronics. Understanding the electro-mechanical behaviors of such material system is crucial for reliable operation of flexible devices under large deformation. In this paper, we performed *in situ* mechanical and electrical tests of ITO thin films with two different thicknesses (200 and 80 nm) deposited on polyimide substrates inside a scanning electron microscope. The crack initiation and propagation, crack density evolution and the corresponding electrical resistance variation were systematically investigated. It was found that cracks initiated at a higher tensile strain level and saturated with a higher density in thinner ITO films. Integrated with a coherently formulated mechanics model, the cohesive toughness and fracture strength of ITO thin films and the ITO/polyimide interfacial toughness were quantitatively determined. The experimentally observed thickness dependence of the saturated crack density in ITO thin films was also quantitatively verified by the model. © *2011 American Institute of Physics*. [doi:10.1063/1.3592341]

I. INTRODUCTION

Flexible electronics, e.g., paper like displays, printable thin-film solar cells, and skinlike smart prostheses, are attracting enormous interests due to their large deformability, light weight, large surface areas, and low cost.[1–4] The desirable attributes of flexible electronics result from new choices of building block materials (e.g., organic/inorganic hybrids) and manufacturing method (e.g., roll-to-roll printing).[1] For example, ITO thin films on polymer substrates are widely used as transparent conductors and interconnects in flexible displays. While compliant polymer substrates can sustain large strain, ITO thin films are brittle and often fracture at small strain. The cracking of ITO conductors and interconnects leads to loss of electrical conductance, posing crucial challenge to the reliability of flexible devices. In this paper, we report a coherent study integrating *in situ* electro-mechanical experiments and mechanics modeling to decipher the failure mechanics of ITO thin films on polyimide substrates under tension. Our *in situ* tensile tests inside a scanning electron microscope (SEM) reveal real time details of crack initiation and propagation, crack density evolution, and associated resistance variations in thin ITO conductors on polyimide substrates. Our mechanics model offers quantitative determination of critical mechanical properties (ITO cohesive toughness, fracture stress, and ITO/polyimide interfacial toughness) from the experimental data and explains the thickness dependence of crack density evolution in ITO conductors.

Fracture of thin brittle films on rigid substrates (e.g., Si) has been a focused topic in the discipline of materials science and mechanics in the past two decades, largely originated from the context of microelectronics.[5–9] These studies shed important lights on but cannot fully capture the characteristics of the fracture mechanisms of thin brittle films (e.g., ITO) on polymer substrates used in flexible electronics. For example, ITO is more than two orders of magnitude stiffer than typical polymers (e.g., polyimide), while electronic materials in microelectronics have comparable stiffness. Furthermore, flexible devices are often subject to deformation (up to 10%) much larger than what traditional microelectronic devices typically undergo (<1%). These two distinctions cause the material response of ITO thin films on polymer substrates different from that of brittle films on rigid substrates, which therefore requires new efforts to describe its characteristics. A growing literature exists on the rupture of thin metal films on polymer substrates.[10–17] Metal film necking and metal/polymer interfacial delamination have been shown as the major fracture mechanisms. Unlike the ductile failure of thin metal films on polymer substrates as a result of diffusive necking, the fracture of brittle ITO thin films on polymer substrates results from channel cracking, which in turn often interplays with the delamination along the ITO/polymer interface. Existing studies on the brittle fracture of ITO thin films on polymer substrates under tension include the fragmentation tests in which the crack density evolution as a function of the applied strain is monitored.[18,19] The cohesive toughness of the ITO films and the adhesive toughness of the ITO/polymer interface can be estimated based on the experimental data from fragmentation tests.[20] The variation of electrical resistance due to ITO cracking has also been studied.[21–23] Other mechanics models investigate the effect of the large film/substrate stiffness ratio on the cracking of thin brittle films on compliant substrates.[24–27]

a)Electronic mail: lit@umd.edu.
b)Electronic mail: jlou@rice.edu.

In this paper, we perform *in situ* mechanical and electrical tests of ITO thin films deposited on polyimide substrates inside SEM, in which both the evolution of the crack density in ITO thin films and the resulting variation of the electrical resistance of the ITO thin films are monitored real time as a function of applied tensile strain. Simultaneous *in situ* mechanical and electrical tests are of particular importance to correlate crack initiation and propagation with its resistance change, and to avoid the unloading-induced partial or full closure of cracks in the ITO thin film in *ex situ* tests. We further conduct mechanics modeling to simulate the tensile failure process of ITO thin films on polymer substrates, and apply the model to the experimental data to compute the critical but hard-to-measure properties, such as the cohesive toughness and fracture strength of the ITO thin films and the adhesive toughness of the ITO/polyimide interface. The mechanics modeling suggests that the saturation of crack density in ITO thin films results from the decrease of the tensile stress in ITO below its fracture strength as the ITO/polyimide interfacial delamination advances, which agrees with experimental observation.

II. MATERIAL AND EXPERIMENTAL METHOD

A. Sample preparation

ITO thin films were deposited on polyimide substrates (Dupont Kapton 50NH, 12.7 μm in thickness) by E-beam evaporation. The resulting ITO/polyimide laminates were then cut into rectangle strip samples for *in situ* tests, with gauge length ~13 mm and width ~3 mm. Mixed ITO powder (In_2O_3 and SnO_2, weight ratio of 90%:10%, density of 7.14 g/cm^3) was used as the evaporation sources in a Sharon E-beam evaporator. The deposition rate was kept at 1~3 Å/s and chamber pressure was at $\sim 1 \times 10^{-5}$ Torr. Before loaded into the chamber, polyimide substrates were cleaned in an ultrasonic cleaner for ten mins with acetone and ethanol and then dried with nitrogen gas. The thickness of ITO thin films were determined by an atomic force microscope (Pico-Plus AFM, Agilent Inc.), using the contact mode. Samples with two ITO film thicknesses (200 nm and 80 nm) were tested in SEM.

B. *In situ* mechanical and electrical tests

The *in situ* tensile tests were performed using a micro-tester (Deben UK, Ltd.) inside the SEM chamber (FEI Quanta 400 high resolution field emission scanning electron microscope, FEI company, Hillsboro, OR). The maximum force and displacement capacities of the micro-tester are 200 N and 10 mm, with resolution of 0.01 N and 0.001 mm, respectively. The uni-axial tensile tests were conducted under displacement control, and the strain rate was controlled to be around 10^{-4}/s. The increase of applied tensile strain was paused at certain preset strain values to allow for high resolution SEM imaging at different locations along the sample length. The electrical resistance of the samples was measured by two point probe method using a Keithley 2000 multimeter during the tensile test.

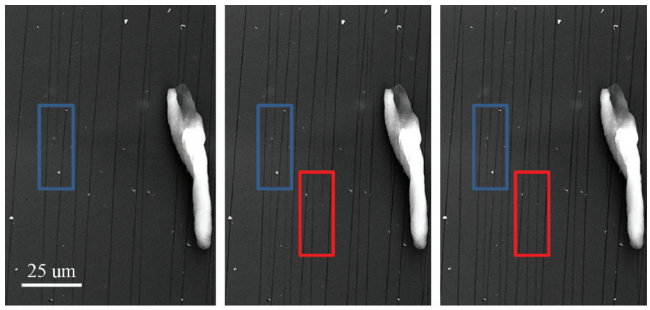

FIG. 1. (Color online) Crack initiation and propagation during *in situ* tensile test. A crack tip was found near the top edge of the blue rectangle box in (a) strain = 3.68% and this crack propagated downward and advanced outside of the same blue rectangle box in (b) strain = 4.70%. Similar phenomena is also shown in the red rectangle box in (b) strain = 4.70% and (c) strain = 5.85%. The dust in the right corner is used as the reference for *in situ* observation.

III. EXPERIMENTAL RESULTS AND DISCUSSION

A. *In situ* SEM observation of crack initiation and propagation in ITO films

From *in situ* SEM observation, the unloaded ITO thin films were smooth, without any appreciable cracks. As the tensile strain increased to a threshold value (e.g., 1.59% for 80 nm thick ITO films), small channel cracks started to initiate at certain locations in the ITO film and then grew along the sample width direction (perpendicular to the tensile load direction). Fig. 1 illustrates the typical process of crack initiation and propagation as the tensile load increases. Here, the ITO film thickness is 80 nm. For example, a crack tip was found near the top edge of the blue rectangle box in Fig. 1(a) at the tensile strain of 3.68% and this crack propagated downward and advanced outside of the same blue rectangle box at the tensile strain of 4.70% [Fig. 2(b)]. Meanwhile, a channel crack not existing in the view of Fig. 1(a) propagated upward with its tip slightly above the top edge of the blue rectangle box in Fig. 1(b). Similar crack propagation is also evident when comparing the red rectangle box in Figs. 1(b) and 1(c), as the tensile strain increased from 4.70% to 5.85%.

B. Crack density evolution and measurement of resulting change in sample electrical resistance

Figure 2 shows a series of snap shots of the polyimide-supported ITO film to illustrate the increasing number of cracks in the film as the tensile load increases. Here the ITO film thickness is 80 nm. At small tensile strain [e.g., 0.55%, Fig. 2(a)], the ITO film remained intact. Above a threshold tensile strain for crack initiation [1.59%, Fig. 2(b)], channel cracks started to emerge in the view. As the tensile strain increased [e.g, Figs. 2(c)–2(e)], more channel cracks initiated and propagated through the sample width. It was found that the channel crack distribution in the ITO film is quite uniform along the sample length direction (also the tensile load direction), suggesting the rather uniform elongation of the polyimide substrate. The sample was further stretched until the polyimide substrate ruptured into two halves. Figure 2(f) shows the ITO fragments near the sample rupture location.

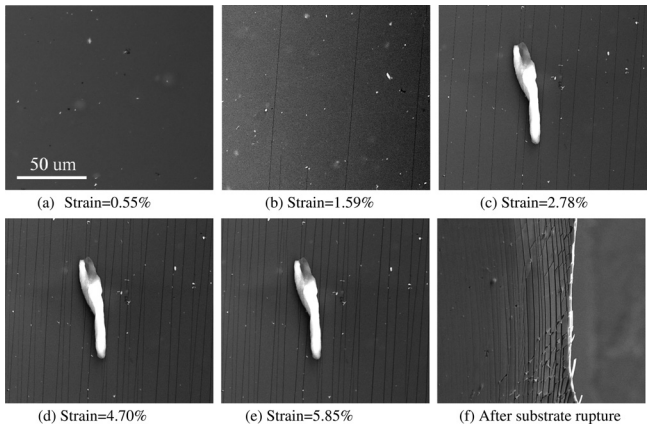

FIG. 2. (a)–(e). Snap shots of polyimide-supported ITO film under increasing tensile strain. Note the onset of channel crack initiation at 1.59% tensile strain (b) and the increasing crack density as the tensile strain increases. No appreciable increase of crack density when tensile strain increases from 4.70% to 5.85% (d)–(e), indicating the saturation of channel cracking in the ITO film. (f). ITO fragments near the sample rupture location. Note, the obvious delamination along the ITO/polyimide interface. Here ITO film thickness is 80 nm.

Note the obvious delamination along the ITO/polyimide interface near the edges of the ITO fragments.

To quantitatively characterize the ITO cracking under tensile strain, we define the *crack density* as the number of channel cracks in ITO film per unit length in the tensile load direction. In all data reported hereafter, the crack density of the samples is calculated as the average of crack density values obtained from at least three SEM images of the cracked ITO thin film in different random locations. Figure 3 plots the crack density in an 80 nm thick ITO film on a polyimide substrate as well as the resulting resistance variation of the ITO thin film as a function of the applied tensile strain. As shown in Fig. 3, once the onset of crack initiation starts, the crack density first increases significantly as the tensile strain increases, and then gradually saturates at about 190 mm^{-1} as the tensile strain approaches to 5.85%. Also evident in Fig. 3, the electrical resistance of the ITO thin film remains nearly unchanged when the applied tensile strain is relatively small. For example, when compared with the as-fabricated ITO film, there is less than 2.5 times increase in resistance for a

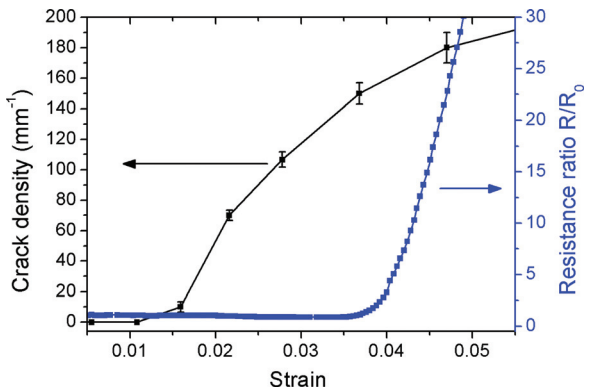

FIG. 3. (Color online) The crack density and the variation of electrical resistance of an 80 nm thick ITO film deposited on polyimide as a function of the applied strain. R_0 denotes the electrical resistance of the unloaded ITO thin film.

tensile strain less than 3%. In other words, the ITO thin film remains electrically conductive when subject to a modest elongation. As the applied tensile strain further increases, the ITO electrical resistance first rises gradually, and then shoots up dramatically as the tensile strain approaches the value at which the crack density saturates. Such a correlation between the evolution of crack density and the change in electrical resistance in the ITO thin film under tension can be explained as follows. At the onset of crack initiation, many channel cracks start to nucleate but have not fully propagate through the whole sample width. As a result, the electrical conductance of the partially cracked ITO film remains nearly unchanged as a current can percolate through the whole ITO conductor. As the applied tensile strain increases modestly, the short channel cracks nucleated in the ITO thin film start to advance through the width of the samples, but the opening displacement of these channel cracks is relatively small, as evident by the rather thin crack lines in the SEM images [e.g., Figs. 2(b) and 2(c)]. When the crack opening is small, the local irregularity of the macroscopically straight channel cracks (e.g., the zigzag grain boundaries in the ITO thin film) may keep the ITO fragments in contact at certain locations in the wake of the channel cracks, and it is also likely that at certain locations the channel cracks have not fully developed to reach the ITO/polyimide interface thus the ITO thin film is not completely fragmentized. As a result, the ITO thin film remains conductive and its electrical resistance only increases modestly. As the applied strain further increases, channel cracks in the ITO thin film are fully developed, resulting in larger cracking opening [as shown by the thicker cracking lines in Figs. 2(d)–2(f)]. Our further measurements of the total crack length and crack opening in the ITO thin film as a function of the applied strain further confirm the above explanation. That is, the total crack length increases drastically at small strains (corresponding to channel crack initiation) and such increases in total crack length diminish significantly (corresponding to the fully developed channel cracks) when the applied strain is beyond about 4% (at which the ITO resistance starts to increase dramatically). Further increase of the ITO resistance is shown to be consistent with the continuously increasing crack opening.

Also as evident in Fig. 2(f) and further predicted in the simulations, the ITO fragments partially delaminate from the polyimide substrate. Consequently, the conductance of the ITO thin film is nearly cutoff. As to be further explained later, the interfacial delamination mitigates the tensile stress transferred from the substrate to the ITO film, therefore prevents further initiation of channel cracks, resulting in the saturation of the crack density.

C. Thickness dependence of crack density in ITO thin films

Figure 4 plots the crack density in the ITO thin films as a function of applied tensile strain for film thickness of 200 nm and 80 nm, respectively. For each thickness, two samples were tested. It was found that the crack initiation in a thicker ITO film occurs at relatively smaller applied tensile strain than that for a thinner ITO film. However, the saturated crack

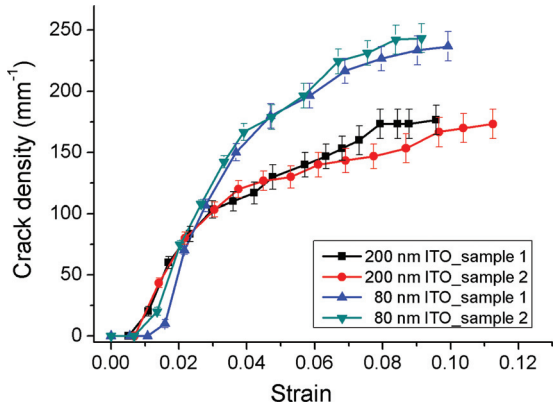

FIG. 4. (Color online) Crack density as a function of applied strain for ITO thin films with thickness of 80 nm and 200 nm, respectively. Two samples were tested for each film thickness.

density of the thicker ITO film is lower than that of the thinner ITO film. Assuming a brittle nature of ITO film fracture, the critical tensile strain to initiate cracking in an ITO thin film scales inversely with the square root of the length of the largest pre-existing defects in the film. For a thicker ITO film, it is more likely to have larger initial defects (e.g., voids, missing grains, or embrittled grain boundary during deposition), and therefore, entails a relatively lower onset strain of crack initiation. The thickness dependence of the crack density will be explained in detail later in Sec. IV through a fracture mechanics analysis.

IV. MECHANICS MODEL AND RESULTS

We next establish a mechanics model to use the *in situ* experimental data of ITO crack density evolution to compute the critical but hard-to-measure properties of the ITO/polymer laminates, such as the cohesive toughness and fracture strength of the ITO films and the adhesive toughness of the ITO/polyimide interface. We also offer a mechanistic understanding of the thickness dependence of the saturated ITO crack density.

A. Simulation model

Figure 5 depicts the finite element simulation model. Under tension, a thin blanket ITO film on a polymer substrate is subject to channel cracking [Fig. 5(a)]. For simplification, we assume the channel cracks in ITO are uniformly spaced (i.e., the crack density is given by $1/s$, where s is the width of ITO fragments). The ITO/polymer laminate is taken to deform under the plane strain conditions. Taking advantage of symmetry we model only a unit cell of the laminate, consisting of a half of the ITO stripe between two neighboring channel cracks and the substrate underneath [Fig. 5(b)]. In the simulation model, the film is a layer with thickness h, and the substrate is a block with thickness $1000h$ and length $s/2$. Symmetric boundary condition is set for the left edge of the unit cell and a horizontal displacement u is set along substrate portion of the right edge of the unit cell. The quantity $2u/s$ defines the applied strain.

Both the ITO film and the polymer substrate are modeled as linear elastic materials with Young's modulus of 140 GPa and 2 Gpa, respectively, and Poisson's ratio of 0.3 and 0.4, respectively. The linear elastic assumption is reasonable for the ITO film but has some limitations for the polymer substrate whose impact on modeling results will be discussed in detail later in the paper.

The channel cracks lead to stress concentration in the substrate near the channel roots, which could be severe enough to cause delamination along the ITO/polymer interface, as also evident in the *in situ* experiments. To simulate the cracking-induced interfacial delamination, the ITO/polymer interface is modeled as an array of nonlinear springs, which is characterized by a tensile and a shear traction-displacement law, with six parameters: interfacial tensile strength σ_n and shear strength σ_s, critical opening displacement δ_n and sliding displacement δ_s, and the areas under the traction-displacement curves Γ_n and Γ_s (i.e., the normal and shear adhesion energy of the ITO/polymer interface, respectively), as illustrated in Fig. 5(c). We assume that $\sigma_n = \sigma_s$, $\delta_n = \delta_s$ and $\Gamma_n = \Gamma_s$. In all simulations, $\sigma_n = 500$ MPa and $\delta_n = 0.5$ nm. The interfacial toughness Γ_n is varied to fit the crack density versus applied strain curve from *in situ* experiments. The ITO/polymer interface is meshed with four-node cohesive elements sharing nodes with the neighboring elements in the film and the substrate. The viscous regularization option in finite element codes ABAQUS is used for the cohesive elements to enhance the computation convergence.

B. Modeling strategy and results

When a freestanding ITO thin film is subject to tension, it fractures by a *single* channel crack running through its width. Supported by a polymer substrate, the tensile fracture of the ITO thin film involves the initiation and propagation

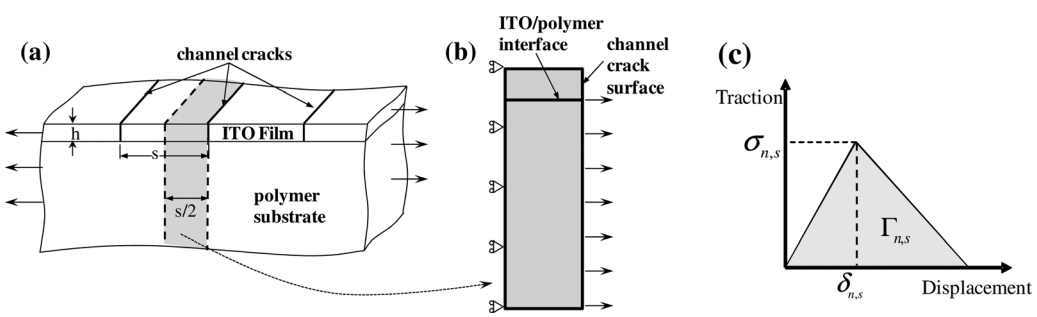

FIG. 5. (a) Schematics of the simulation model. (b) Unit cell used in finite element simulation. (c) The traction-displacement laws used to model the ITO/polymer interface.

of *multiple* channel cracks, and the subsequent increase and saturation of the crack density as the applied tension increases, as observed in experiments. The increase of crack density is due to the transfer of tensile load from the polymer substrate to the ITO film through the interface. The brittle nature of the channel cracks in ITO thin film leads to severe stress concentration in the substrate near the channel roots that can cause delamination along the ITO/polymer interface. As the delamination initiates and propagates along the interface, the tensile load transferred from the polymer substrate to the ITO film decreases. If the delamination length is sufficiently large, the maximum tensile stress in the ITO film drops below the ITO fracture strength. As a result, no further channel cracks can be initiated in the ITO film. In other words, the crack density in the ITO film saturates.

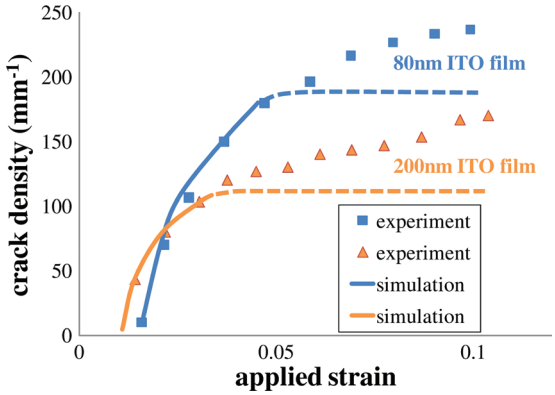

FIG. 6. (Color online) The crack density vs applied strain curves from the best-fit simulations and experiments, for ITO film thickness of 80 nm and 200 nm, respectively.

1. ITO/polyimide interfacial toughness and ITO fracture strength

Based on such an understanding, we apply the following modeling strategy in the simulations. For a given crack density versus applied strain curve from *in situ* experiments (e.g., Fig. 4), the crack density corresponding to the channel crack onset strain (e.g., 10/mm at 1.59% for 80 nm thick ITO film) defines a FEM simulation model with width of 50 μm [e.g., Fig. 5(b)]. An ITO/polymer interfacial toughness (i.e., Γ_n) is assigned for the traction-displacement law of the interface. This unit cell model is stretched to the channel crack onset strain. The maximum tensile stress in the ITO, which occurs at the ITO portion of the left edge of the unit cell, is obtained. Given the brittle nature of the fracture of the ITO thin film, such a tensile stress indicates the ITO fracture strength, above which channel cracking occurs. A series of FEM unit cell models are then built with widths corresponding to the crack density values in the same experimental curve. Each simulation model is then stretched to a certain applied strain at which the maximum tensile stress in the ITO thin film reaches the ITO fracture strength determined from the first simulation model (i.e., right before next channel crack initiates). Although the subsequent crack initiation is not simulated directly, the modeling strategy adopted here can still reasonably capture the underlying failure mechanism, given that the brittle nature of the crack initiation and propagation (e.g., as shown in Fig. 1). The corresponding crack density versus applied strain curve based on the above simulations is then plotted together with that from the *in situ* experiment for comparison. The value of Γ_n in the traction-displacement law of the ITO/polyimide interface is then varied, and the above simulation procedure is repeated until the best fit between the simulation and experiment curves is reached. The corresponding value of Γ_n and maximum tensile stress in the ITO thin film are defined as the ITO/polyimide interfacial toughness and the ITO fracture strength, respectively.

Figure 6 plots the crack density versus applied strain curves from the best-fit simulations and experiments, for ITO film thickness of 80 nm and 200 nm, respectively. The ITO/polyimide interfacial toughness and the ITO fracture strength obtained from the best fit simulations are 9.5 J/m^2 and 2.4 GPa for 80 nm thick ITO film, and 10.8 J/m^2 and 1.7 GPa for 200 nm thick ITO film, respectively. As shown in Fig. 6, the simulation curves can fit the experiment curves quite well until a certain applied strain. When the applied strain further increases, the maximum tensile stress in the ITO film cannot reach the ITO fracture strength, therefore no further channel crack can be initiated. In this sense, the simulation model underestimates the saturated crack density. Such a discrepancy in saturated crack density between the modeling and the experiment results can be attributed to the assumption of elastic behavior of the polymer substrate. In reality, the polymer substrate yields and deforms plastically if the applied tensile strain exceeds a critical value. The linear elastic assumption for the polymer leads to an overestimated tensile stress in the substrate. As a result, under a given applied tension, the length of the delamination along the ITO/polymer interface is also overestimated due to the increased stress concentration at the delaminating front. Consequently, the tensile stress transferred to the ITO thin film is underestimated, leading to a prediction of saturated crack density lower than that measured in the *in situ* experiments. Nonetheless, those predicted values from the simulations offer estimates of the lower bounds of the ITO/polyimide interfacial toughness and ITO fracture strength, which agree with the results from other recent experiments.

Figure 7(a) plots the variation of the tensile stress in the 80 nm thick ITO thin film as a function of the relative location in a unit cell model, at various applied strains. When the applied strain is small, the distribution of the tensile stress is rather uniform in majority part of the ITO thin film except the portion near the channel crack. As the applied strain increases, interfacial delamination initiates and propagates. As a result, the tensile stress transferred to the ITO thin film is reduced, leading to a rather nonuniform distribution of the tensile stress in the ITO thin film, with the highest level at the center of the ITO fragment and gradually diminishing to zero in the delaminated portion. Figure 7(b) further plots the delamination length normalized by the ITO fragment width as a function of applied strain, for both 80 nm and 200 nm thick ITO films, respectively, which clearly shows the advance of interfacial delamination, and therefore the underlying mechanism for the saturation of crack density in polymer-supported ITO thin films under tension.

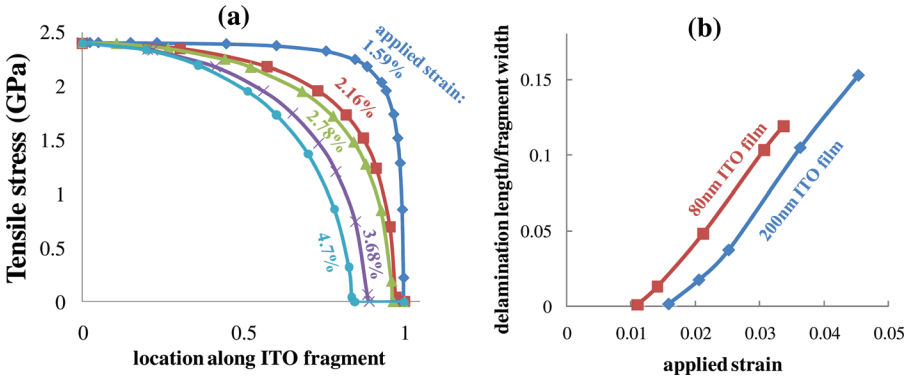

FIG. 7. (Color online) (a) The variation of the tensile stress in the 80 nm thick ITO thin film as a function of the relative location in a unit cell model, at various applied strains. For the horizontal axis, zero denotes the center of the ITO fragment and one denotes the right edge of the ITO fragment (i.e., the channel crack surface). (b) The delamination length normalized by the ITO fragment width as a function of applied strain, for both 80 nm and 200 nm thick ITO thin films, respectively.

2. ITO cohesive toughness

Given the brittle nature of the ITO thin film fracture, the cohesive toughness of the ITO thin film is defined as the energy required for propagating channel crack to generate new crack surface of unit area. The detailed shape and deformation state near the channel crack front can be rather complicated, and hard to predict. By contrast, far ahead and far behind the channel crack front, the structure can be taken to deform under the plane strain conditions. Since both ITO and polymer are assumed to be linearly elastic at the channel crack onset strain, the driving force for the channel cracking can be calculated by the elastic energy stored in a slice of ITO/polymer laminate of unit thickness far ahead of the channel crack front minus the elastic energy stored in a slice of ITO/polymer laminate of unit thickness far behind the channel crack front. In the simulation, the widths of these two slices of ITO/polymer laminate are set to be the reciprocal of the crack density corresponding to the crack onset strain in the *in situ* experiment. The slice far ahead of the channel crack front has a continuous ITO thin film, while the slice far behind has a channel crack in the middle of the ITO thin film. Each slice is subject to an applied strain equal to the crack onset strain, and the resulting strain energy is calculated in ABAQUS. Applying the above simulation strategy to the experiment results, we obtain a cohesive toughness of 42.0 J/m^2 for ITO films with thickness of 80 nm and 40.4 J/m^2 for ITO films with thickness of 200 nm. These values roughly agree with the results from other recent studies.[20]

3. Mechanistic understanding of thickness dependence of saturated crack density in ITO film

The thickness dependence of the saturated crack density in polymer supported brittle films has been observed in previous studies.[28] A few mechanics models have been considered to explain such thickness dependence.[29] A consideration of the force balance of an ITO fragment at the saturation limit gives $\tau = 2h_{ITO}\sigma/s_{cr}$, where τ is the interfacial shear stress, h_{ITO} is the ITO film thickness, σ is the tensile stress in ITO film and s_{cr} is a length close to the ITO fragment width at the saturation limit (i.e., $1/s_{cr}$ approximately denotes the saturated crack density). A fracture mechanics based dimensional consideration leads to $\sigma \propto \sqrt{\Gamma_{ITO}/h_{ITO}}$, where Γ_{ITO} is the cohesive toughness of the ITO film. Given that the same fabrication conditions in depositing ITO films of different thickness on the same polymer substrate, it is reasonable to assume similar interfacial properties in different samples (e.g., as evident by the similar interfacial toughness values predicted above). In other words, the interfacial shear stress τ remains to be constant. The above analysis yields that the thickness dependence of the saturated crack density takes the form of $\sqrt{\Gamma_{ITO}h_{ITO}}/s_{cr} \approx$ constant. Using the ITO cohesive toughness obtained in Section IV B 2 and the saturated crack density data from *in situ* experiments, the value of $\sqrt{\Gamma_{ITO}h_{ITO}}/s_{cr}$ for $h_{ITO} = 80$ nm agrees with that for 200 nm within about 10%. This good agreement confirms the above mechanics understanding of the thickness dependence of the saturated crack density in polyimide supported ITO thin films.

V. CONCLUSIONS

In summary, we reported a coherent study integrating *in situ* electro-mechanical experiments and mechanics modeling to decipher the failure mechanics of ITO thin films on polyimide substrates under tension. Our *in situ* tensile tests inside SEM reveal real time details of crack initiation and propagation, crack density evolution, and associated electrical resistance variations in thin ITO conductors on polyimide substrates. The corresponding mechanics model offers quantitative determination of critical mechanical properties (ITO cohesive toughness, fracture stress, and ITO/polyimide interfacial toughness) from the experimental data and explains the experimentally observed thickness dependence of crack density evolution in ITO conductors. While the understanding from the two dimensional model used in this paper sheds light on the governing failure mechanisms of the ITO/polymer structure (i.e., ITO channel cracking versus ITO/polymer interfacial delamination), further studies such as three dimensional modeling are necessary to capture the detailed interplay of these two governing failure mechanisms.

ACKNOWLEDGMENTS

This work was supported by National Science Foundation (NSF) through collaborative research grants (Grant Nos. 0928278 and 0928297). T.L. also acknowledges the support of NSF through Grant No. 0856540. J.L. acknowledges the support of AFOSR through YIP award FA9550-09-1-0084.

The authors thank the Dupont company for providing the polyimide samples used in this work.

[1]G. P. Crawford, *Flexible Flat Panel Displays* (Wiley, Hoboken, 2005).
[2]C. J. Brabec, Sol. Energy Mater. Sol. Cells **83**, 273 (2004).
[3]S. Wagner, S. Lacour, J. Jones, P.-H. Hsu, J. Sturm, T. Li, and Z. Suo, Physica E **25**, 326 (2004).
[4]T. Someya, T. Sekitani, S. Iba, Y. Kato, H. Kawaguchi, and T. Sakurai, PNAS **101**, 9966 (2004).
[5]J. L. Beuth, Int. J. Solids Struct. **29**, 1657 (1992).
[6]J. W. Hutchinson and Z. Suo, Adv. Appl. Mech. **29**, 63 (1992).
[7]Q. Ma, J. Mater. Res. **12**, 840 (1997).
[8]T. Y. Tsui, A. J. McKerrow, and J. J. Vlassak, J. Mater. Res. **20**, 2266 (2005).
[9]X. H. Liu, M. W. Lane, T. M. Shaw, and E. Simonyi, Int. J. Solids Struct. **44**, 1706 (2007).
[10]S. L. Chiu, J. Leu, and P. S. Ho, J. Appl. Phys. **76**, 5136 (1994).
[11]B. E. Alaca, M. T. A. Saif, and H. Sehitoglu, Acta Mater. **50**, 1197 (2002).
[12]M. R. Begley, O. N. Scott, M. Utz, and H. Bart-Smith, Appl. Phys. Lett. **95** 231914 (2009).
[13]T. Li, Z. Huang, Z. Suo, S. Lacour, and S. Wagner, Appl. Phys. Lett. **85**, 3435 (2004).
[14]T. Li, Z. Huang, Z. Xi, S. Lacour, S. Wagner, and Z. Suo, Mech. Mater. **37**, 261 (2005).
[15]Z. Zhang and T. Li, Scr. Mater. **59**, 862 (2008).
[16]N. S. Lu, X. Wang, Z. G. Suo, and J. Vlassak, Appl. Phys. Lett. **91**, 221909 (2007).
[17]N. Lu, X. Wang, Z. Suo, and J. Vlassak, J. Mater. Res. **24**, 379 (2009).
[18]G. Rochat, Y. Leterrier, P. Fayet, and J. A. E. Manson, Thin Solid Films **437**, 204 (2003).
[19]Y. Leterrier, L. Medico, F. Demarco, Manson, U.Betz, M. F. Escola, Kharrazi, and F. Atamny, Thin Solid Films **460**, 156 (2004).
[20]N. E. Jansson, Y. Leterrier, L. Medico, and J. A. E. Manson, Thin Solid Films **515**, 2097 (2006).
[21]D. R. Cairns, R. P. Witte, D. K. Sparacin, S. M. Sachsman, D. C. Paine, G. P. Crawford, and R. R. Newton, Appl. Phys. Lett. **76**, 1425 (2000).
[22]D. R. Cairns and G. P. Crawford, Proc. IEEE **93**, 1451 (2005).
[23]K. A. Sierros, N. J. Morris, K. Ramji, and D. R. Cairns, Thin Solid Films **517**, 2590 (2009).
[24]J. M. Ambrico and M. R. Begley, Thin Solid Films **419**, 144 (2002).
[25]J. J. Vlassak, Int. J. Fract. **119**, 299 (2003).
[26]H. X. Mei, Y. Y. Pang, and R. Huang, Int. J. Fract. **148**, 331 (2007).
[27]Z. Jia, M. B. Tucker, and T. Li, Comp. Sci. Tech. **71**, 365 (2011).
[28]N. E. Jansson, Y. Leterrier, and J. A. E. Manson, Eng. Fract. Mech. **73**, 2614 (2006).
[29]Y. Leterrier, Prog. Mater. Sci. **48**, 1 (2003).